COMMENT

The motion of an arbitrarily rotating spherical projectile and its application to ball games

To cite this article: Garry Robinson and Ian Robinson 2013 *Phys. Scr.* **88** 018101

View the article online for updates and enhancements.

The motion of an arbitrarily rotating spherical projectile and its application to ball games

Garry Robinson[1] and Ian Robinson[2]

[1] School of Physical, Environmental and Mathematical Sciences, The University of New South Wales, Australian Defence Force Academy, Canberra, ACT 2600, Australia
[2] Centre for Research on Education Systems, Melbourne Graduate School of Education, The University of Melbourne, Melbourne, VIC 3010, Australia

E-mail: g.robinson@adfa.edu.au and robbo@unimelb.edu.au

Abstract

In this paper the differential equations which govern the motion of a spherical projectile rotating about an arbitrary axis in the presence of an arbitrary 'wind' are developed. Three forces are assumed to act on the projectile: (i) gravity, (ii) a drag force proportional to the square of the projectile's velocity and in the opposite direction to this velocity and (iii) a lift or 'Magnus' force also assumed to be proportional to the square of the projectile's velocity and in a direction perpendicular to both this velocity and the angular velocity vector of the projectile. The problem has been coded in MATLAB and some illustrative model trajectories are presented for 'ball-games', specifically golf and cricket, although the equations could equally well be applied to other ball-games such as tennis, soccer or baseball.

Spin about an arbitrary axis allows for the treatment of situations where, for example, the spin has a component about the direction of travel. In the case of a cricket ball the subtle behaviour of so-called 'drift', particularly 'late drift', and also 'dip', which may be produced by a slow bowler's off or leg-spin, are investigated. It is found that the trajectories obtained are broadly in accord with those observed in practice. We envisage that this paper may be useful in two ways: (i) for its inherent scientific value as, to the best of our knowledge, the fundamental equations derived here have not appeared in the literature and (ii) in cultivating student interest in the numerical solution of differential equations, since so many of them actively participate in ball-games, and they will be able to compare their own practical experience with the overall trends indicated by the numerical results.

As the paper presents equations which can be further extended, it may be of interest to research workers. However, since only the most basic principles of fundamental mechanics are employed, it should be well within the grasp of first year university students in physics and engineering and, with the guidance of teachers, good final year secondary school students. The trajectory results included may be useful to sporting personnel with no formal training in physics.

PACS numbers: 45.20.D−, 45.40.Gj, 01.80.+b, 02.60.Lj

(Some figures may appear in colour only in the online journal)

S Online supplementary data available from stacks.iop.org/PhysScr/88/018101/mmedia

1. Introduction and background information

The subject of projectile motion has been studied for many centuries and, drawing on fields as diverse as mechanics and fluid dynamics, the subject is relatively complicated, both from the physical and mathematical point of view. It is only with an understanding of the physical principles involved, that one can fully appreciate the complexities in the mathematical formulation of the problem, and also realistically interpret the predicted trajectories. Accordingly, in the interests of the reader not familiar with projectile motion, we have attempted to make this paper as self contained as possible, in order to render it accessible and useful to the widest range of readers.

The present paper may be related to our recent study of a pilot ejecting from a fighter aircraft (Robinson and Jovanoski 2010), the aim of that paper being to see under what conditions impact with the rear vertical stabilizer might occur. After ejection the pilot's trajectory is determined by similar forces to those involved in the present study. The paper may also be useful as a teaching aid, in a similar manner to our previous paper in this journal on radiative transfer in multiple isothermal circumstellar dust shells (Towers and Robinson 2009).

We begin with a detailed introduction to projectile motion, including a discussion of the important physical principles involved.

1.1. Historical perspective

The study of projectile motion probably had its origins in military applications. The simplest approach to finding the trajectory of arbitrarily shaped projectiles is to neglect the effects of the Earth's atmosphere (i.e. the projectile is assumed to be in a vacuum) and consider gravity as the only force. In this case, at least for short paths where the Earth's curvature and rotation can be neglected, there is a simple analytic solution and the trajectory is a parabola. The detailed treatment of this situation is regarded as mandatory in virtually all first year physics texts (e.g. Giancoli 2009, Serway and Jewett 2010, Halliday *et al* 2011, Young and Freedman 2012, Knight 2013). Once any forces other than gravity are included, obtaining an analytic solution becomes increasingly more difficult and usually involves making simplifying assumptions.

The Earth's atmosphere introduces two extra forces, a *drag* force and, if the projectile is spinning, a second force traditionally called the *lift* force, although it does not always produce actual 'lift'. Sir Isaac Newton (1672) himself was first to record the latter effect and gave a qualitative explanation of the curved flight of a spinning tennis ball, based on the interaction of the spinning ball with the atmosphere. Magnus (1853) was the first to introduce a mathematical description of this effect and so the lift force is often referred to as the Magnus force. Both of these forces, at least in elementary treatments, are usually assumed to be proportional to V^2, where V is the magnitude of the projectile velocity, with the drag force acting in the opposite direction to the velocity vector $\vec{V}$, and the lift force acting perpendicular to it[3]. If the Earth's rotation is taken into account, the two inertial

forces, the centrifugal force and the Coriolis force (see e.g. McCuskey 1959, French 1971, Scorer 1997) also play a major role for large distances (e.g. for ballistic missiles)[4].

Over the years many texts on mechanics have discussed projectile motions, some examples being Timoshenko and Young (1948), Housner and Hudson (1959) and the highly respected work of Synge and Griffith (1959). These texts demonstrate some of the approximations that have been made in order to obtain an analytic solution. For a state-of-the-art treatment, however, one must look to specialized books on Exterior Ballistics (sometimes called External Ballistics)[5], the study of exterior ballistics itself in fact dating back over many centuries. Some noteworthy texts in this category include that of Moulton (1926), whose work benefited from experiences of the first World War, and McShane *et al* (1953), written with the experience of the second World War. Recent works include that of Klimi (2008) and Carlucci and Jacobson (2008), both of these books having the benefit of the authors' military experience.

As foreshadowed above, a detailed treatment of projectile motion requires a consideration of fluid dynamics, and especially the behaviour of the fluid in the immediate vicinity of the projectile—the 'boundary layer'. The complexity of the boundary layer may be gauged from an examination of the definitive textbook on the subject by Schlichting and Gersten (2000).

1.2. Spherical projectiles in ball-games

In the special case where the projectile is *spherical*, the problem becomes significantly less complicated and well within the grasp of the non-specialist since, because of the symmetry of the projectile, one does not have to deal with the complexities of 'yaw' and 'pitch'. The review by Mehta (1985) summarizes the aerodynamics of spherical projectiles ('balls') that are used in sport, and provides an extensive list of references. A number of books have appeared over the years treating the motion of such projectiles as used in 'ball-games'. These include the works of Daish (1972), Hart and Croft (1988), de Mestre (1990) as well as the extensive collection of original papers edited by Armenti (1992).

Although many of the works on ball-games include spin of the projectile and hence the lift force, in virtually all cases they limit themselves to the case of the spin axis being *perpendicular* to the plane of the projectile velocity vector, $\vec{V}$, and more specifically to the cases of pure top-spin, pure under-spin or pure side-spin[6]. A notable exception is the

---

[3] A complete list of symbols used in this paper, together with their meanings, is given in appendix A, table A.1.

[4] Although the inertial forces may not be of significance in 'ball-games', it is interesting to note that the effect of the Coriolis force on the small scale has been investigated since the time of Newton via the study of the deviation of the path from the vertical of a freely falling object. In the early 20th century Hall (1903a, 1903b) found, in a very precise experiment involving 948 trials, that for a latitude of $42°$ N, an object allowed to fall vertically through a distance of 23 m suffered, on average, an eastward deflection of 1.49 mm and a southerly deflection of 0.050 mm. The eastward deflection is clearly due to the Coriolis force, the theoretical value being 1.79 mm. (Regarding the accuracy of the easterly deflection measurement, Hall wrote: 'I attach but little significance to this discrepancy ...'.) Many other observers have in fact also reported the small southerly (in the northern hemisphere) deflection, but its exact origin appears to be an open question (see also French 1971, p 552).

[5] The term 'Exterior' has its origins in projectiles fired from guns, and is used to describe the situation after the projectile has left the gun-barrel.

[6] An indication of the spin terminologies used in this paper for golf and cricket may be found in section 7, table 2.

work of Spathopoulos (2009), who used a spreadsheet model to investigate the motion of a spinning soccer ball. Although he restricted the spin axis to being confined to a plane perpendicular to the plane of the projectile initial velocity vector, its angle within that plane was unrestricted, corresponding to a combination of, in general, both under-spin (or top-spin) and side-spin. The above assumptions are entirely reasonable for describing the motion of a soccer ball, bearing in mind its flat trajectory and the mechanics involved in kicking the ball. However, for other ball-games, for example spin bowling in cricket, the assumptions are not so valid.

While a ball initially with top-spin, for example, will always possess only top-spin, provided it retains its spin, the situation can be more complicated for other spin directions. For example, a ball projected horizontally with the spin axis in the same direction as the initial velocity vector will, by symmetry, initially have no lift force, but as the velocity develops a downward component under gravity, a side-ways lift force will be generated. Such a situation is directly relevant to leg-spin and off-spin bowling in cricket. The investigation of such problems clearly necessitates consideration of the general case of a spin about an *arbitrary* axis.

Spin about an *arbitrary* axis is significantly more difficult to treat and, given that we have not seen it discussed in the literature, forms a key part of the new material and insights presented in this paper. The mathematical formulation to be presented here, although an approximation to the true physical situation, is realistic enough to provide physically reasonable answers, and is well within the grasp of most undergraduate students studying applied mathematics, physics or engineering.

1.3. Physical origin of the Magnus force

An examination of a number of modern first year university physics textbooks reveals that the Magnus effect is rarely treated, whereas in older texts (see e.g. Weidner and Sells 1973, Marion and Hornyak 1982) a brief discussion was often presented. In this section we include a simplified account of the physics underlying the Magnus force, partly because of its direct relevance to the subject at hand and partly because the physics underlying the effect itself may motivate students.

If a sphere is moving through a fluid, such as air, it is subject to a drag force, $\vec{\mathbf{F}}_D$, which, by symmetry, is in the opposite direction to the motion. If the sphere is spinning it is also subject to a second force, the lift or Magnus force, $\vec{\mathbf{F}}_L$. Figure 1 shows a schematic diagram of a sphere moving to the right with a velocity relative to the air of $\vec{\mathbf{V}}$, and spinning in an anti-clockwise sense with angular velocity $\vec{\boldsymbol{\omega}}$ about an axis perpendicular to $\vec{\mathbf{V}}$. This corresponds to the case of 'under-spin'. From the point of view of the forces and physical processes involved, this situation is identical to the wind-tunnel simulations in which it is more convenient experimentally to have the spinning sphere in a fixed position and the air-stream moving with velocity $\vec{\mathbf{V}}$ in the opposite direction, i.e. to the left.

Two types of fluid flow can occur in the *boundary layer*, laminar flow (also called streamline flow) or turbulent flow. (The downstream wake may also have extreme cases of
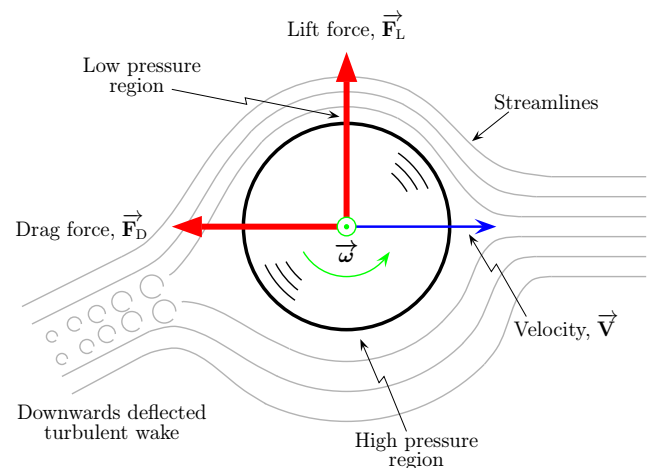
Figure 1. Very much simplified schematic diagram showing the streamlines around a rotating sphere under the conditions of a laminar boundary layer, a condition which is often, but certainly *not* always fulfilled in the case of 'ball-games'. For the case shown of *under-spin*, as is often appropriate to golf, there is a high fluid velocity and thus a low pressure region above the sphere, a low fluid velocity and hence a high pressure region below the sphere, leading to an *upward* lift force, $\vec{\mathbf{F}}_L$. The direction of $\vec{\mathbf{F}}_L$ is perpendicular to both the velocity vector, $\vec{\mathbf{V}}$, and the angular velocity vector, $\vec{\boldsymbol{\omega}}$, the latter being out of the plane of the paper. Note that the streamlines are more closely spaced above the sphere than below, and the turbulent air-stream wake is directed downwards, as demanded by conservation of momentum. The drag force, $\vec{\mathbf{F}}_D$, is in the opposite direction to $\vec{\mathbf{V}}$.

laminar or turbulent flow.) Figure 1 shows the situation for laminar flow in the boundary layer, in which the streamline pattern is stable. It may be seen that, on the top of the sphere the sphere's rotational motion is in the same direction as that of the air velocity relative to the sphere, and thus aids the flow and *increases* the flow velocity. On the other hand, at the bottom of the sphere the rotational motion opposes the air velocity and thus *decreases* its velocity. According to Bernoulli's equation (see e.g. Halliday *et al* 2011, pp 374–7), in regions of the fluid where the velocity is low, the pressure is high, and vice versa. Thus, there is a low pressure region at the top of the sphere and a high pressure region at the bottom of the sphere, leading to an *upward* Magnus force. Note also that the streamlines are dragged around with the spinning sphere and the turbulent fluid wake behind the sphere is deflected *downwards*, as it must be for momentum to be conserved.

The Magnus effect is responsible for the lift produced in an aerofoil, as employed in the wing of an aircraft. The shape of the wing is such that air flows faster over the upper surface of the wing than the lower surface, leading to a lower pressure above the wing than below it and hence an upward lift force.

In reality, the situation is much more complicated than that described above because the fluid flow in the boundary layer can become turbulent rather than laminar. The roughness of the sphere's surface, and certainly the presence of the 'seam' on a cricket ball, can dramatically influence when the transition from laminar to turbulence in the boundary layer occurs, and hence the size of the lift force. Excellent wind-tunnel photographs of flow patterns around a range of objects, obtained under a variety of conditions and which

reveal the complexity of the situation, may be found in Brown (1971) and Van Dyke (1982)[7].
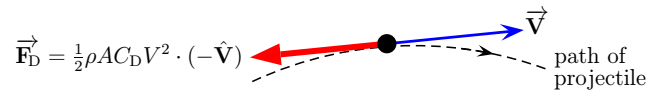
If the flow is turbulent in the boundary layer, the boundary layer clings to the ball further around on the downstream side (i.e. separation is *delayed* as a result of turbulence) leading to a smaller wake and thus a smaller drag force than in the laminar case. (This is why dimpled golf balls fly further than smooth ones, the dimples promoting turbulence.) Furthermore, under certain conditions it is possible for the fluid flow to be turbulent in the boundary layer on the side of the ball where the spin motion opposes the fluid flow (i.e. the low fluid velocity/high pressure side, where the relative velocity of the ball and fluid is largest) and laminar on the side where the spin motion aids the fluid flow (i.e. the high fluid velocity/low pressure side). If this occurs, since the turbulent boundary layer clings further around the ball, the wake is deflected towards the high velocity/low pressure side, i.e. *opposite* to that shown in figure 1. This gives rise to the so-called *negative* Magnus effect, where the Magnus force reverses in direction.

The negative Magnus effect has certainly been observed with *smooth* golf balls, where a ball struck with under-spin and normally subject to an upward lift force can suddenly plummet into the ground (Daish 1972, p 140). The negative Magnus effect was also found by Briggs (1959) to occur for smooth Bakelite balls under certain conditions. In the context of fast bowling in cricket, 'reverse swing' (as opposed to side-ways movement due to spin) is now-days often observed. While not due to the Magnus force because the ball may or may not be spinning, it is similar in the sense that the direction of the sideways movement can reverse as a result of different conditions in the boundary layer and hence the type of fluid flow. In turn this may be influenced by such things as the state of the ball's surface, the condition of the seam, the ball speed and the prevailing atmospheric conditions.

1.4. Numerical solutions and simulations

Since the equations of motion governing the trajectory of a rotating spherical projectile in the general case have no analytic solution, they must be solved numerically. Simulation routines for solving *coupled* partial and/or ordinary differential equation systems date back to the late 1960s or early 1970s. One such package was FORSIM, produced by Carver and his co-workers at the Canadian Chalk River Nuclear Laboratories (Carver 1979). This was written in FORTRAN, and the user had to supply an 'UPDATE' subroutine appropriate to the particular problem at hand which was incorporated in FORSIM. The successful use of FORSIM did require some thought and computational skill on the part of the user. We in fact tackled the present problem some time ago, and formulated it in FORTRAN using FORSIM, but it was documented only in an internal report (Robinson 1984). The current paper draws on that experience.

In more recent years, with the advent of packages such as MATLAB, the numerical solution of differential equation systems has become almost routine, even for students with limited mathematical and computational knowledge. As such

---

[7] A sample of these photographs may be found in the paper *Wind Tunnel Photographs* by Rod Cross at the website http://www.physics.usyd.edu.au/~cross/TRAJECTORIES/Fluidflow Photos.pdf.

$$\vec{\mathbf{F}}_D = \tfrac{1}{2}\rho A C_D V^2 \cdot (-\hat{\mathbf{V}})$$

Figure 2. The drag force, $\vec{\mathbf{F}}_D$ (represented by the broad line with the closed arrow head) acting on a sphere travelling with velocity $\vec{\mathbf{V}}$ relative to the air (represented by the fine line with the open arrow head) is assumed to act in the direction of $-\vec{\mathbf{V}}$ and to be proportional to V^2.

one may develop the relevant equations with some confidence that the equations themselves, and the thought of their numerical solution, will not intimidate the average student.

1.5. Structure of the paper

In this paper the equations of motion governing the trajectory of a spherical projectile, *rotating about an arbitrary axis* in the presence of an *arbitrary wind* are developed. The forces acting on the projectile will be assumed to be: (i) gravity, (ii) a drag force and (iii) a lift or Magnus force. The lift force will be assumed to depend on the angular velocity, ω, in a known way. The equations will be solved numerically using MATLAB and the solutions used to produce illustrative model trajectories for both golf and cricket.

The paper is structured as follows. In section 2 we document the assumptions regarding the drag force (section 2.1) and the lift force for spin about an arbitrary axis (section 2.2) and in section 3 we introduce the effect of a wind. In section 4 we develop the equations of motion and in section 5 we perform some checks of these equations of motion by reducing them to simple well-known situations. In section 6 (and appendix B) we give some details of the MATLAB code and in section 7 we present a number of illustrative model trajectories for golf and cricket. Finally, in section 8 we summarize this work and its principal conclusions, and list some possible extensions. Appendix A contains a list of symbols used throughout the paper.

2. Assumptions regarding the drag and lift forces

In this section we document in some detail the assumptions that have been made regarding the nature of the drag and lift forces, so that readers may judge for themselves their appropriateness, and modify them if they desire (e.g. by varying the velocity and/or angular velocity dependence of the two forces).

2.1. The drag force

If the projectile has a velocity $\vec{\mathbf{V}}$ *relative to the air*, the drag force, $\vec{\mathbf{F}}_D$, is assumed to be in the direction opposite to $\vec{\mathbf{V}}$ and proportional to V^2 where $V = |\vec{\mathbf{V}}|$, as shown in figure 2. The magnitude of the drag force is usually written as

$$F_D = |\vec{\mathbf{F}}_D| = \tfrac{1}{2}\rho A C_D V^2, \tag{1}$$

where ρ is the air density, A is the cross-sectional area of the spherical projectile, C_D is the (dimensionless) drag coefficient and V is the projectile's velocity relative to the air (see e.g. Daish 1972, Hart and Croft 1988, de Mestre 1990).
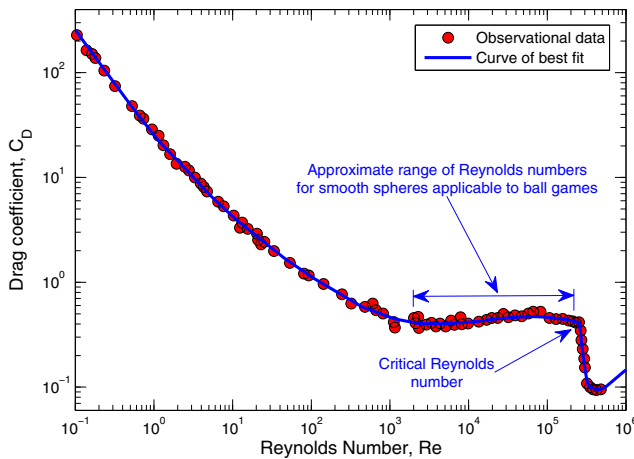
Equation (1) may be written in vector form as

$$\vec{\mathbf{F}}_D = \tfrac{1}{2}\rho A C_D V^2 \cdot (-\hat{\mathbf{V}}) = \tfrac{1}{2}\rho A C_D V \cdot (-V\hat{\mathbf{V}}), \tag{2}$$

where $\hat{\mathbf{V}}$ is a unit vector in the direction of $\vec{\mathbf{V}}$.

Figure 3. The variation of the drag coefficient, C_D, with the Reynolds number, $Re = Vd/\nu$, for *smooth* spheres, the curve representing the best fit to experimental data obtained by a variety of workers. For Re in the range approximately 10^3–3×10^5, C_D is approximately constant, having a value of about 0.45. At the critical Reynolds number of about 3×10^5, C_D decreases abruptly by a factor of about 5 as the boundary layer undergoes a transition from laminar to turbulent flow. (The diagram is based on figure 1.19 of Schlichting and Gersten (2000), with some additions, and this definitive text may be consulted for further details. Complete information on the sources of the original data is given in Schlichting (1979).)

Hence

$$\vec{\mathbf{F}}_D = -\tfrac{1}{2}\rho A C_D V \cdot \vec{\mathbf{V}}. \tag{3}$$

The drag coefficient C_D is in fact dependent on V. The flow pattern around objects moving through a fluid is usually characterized by a dimensionless number proportional to the velocity known as the Reynolds number, Re[8]. The variation of the drag coefficient with the Reynolds number for *smooth* spheres is shown in figure 3. It may be seen that for Re varying between about 10^3 and 3×10^5, C_D remains constant at approximately 0.45. For a cricket ball[9], assumed to behave as a smooth sphere, $Re = 10^3$ corresponds to $V \approx 0.21 \, \mathrm{m \, s^{-1}} \approx 0.76 \, \mathrm{km \, h^{-1}}$ and $Re = 3 \times 10^5$ corresponds to $V \approx 64 \, \mathrm{m \, s^{-1}} \approx 230 \, \mathrm{km \, h^{-1}}$. For tennis and golf balls, again assumed to behave as smooth spheres, the corresponding speeds are approximately 0.87 and $261 \, \mathrm{km \, h^{-1}}$, and 1.46 and $394 \, \mathrm{km \, h^{-1}}$ respectively. Thus for the applications of interest here C_D will be assumed to be constant at 0.45 and hence F_D will be assumed to be proportional to V^2.

It may be noted that most balls used in ball games are *not* smooth spheres and thus figure 3 is not strictly applicable. Little data are available for non-smooth spheres and few data, even for smooth spheres, exist far beyond the critical Reynolds number at which the abrupt reduction in C_D occurs

[8] The Reynolds number is defined by $Re = Vd/\nu$. Here d is a characteristic size of the object (the diameter in the case of a spherical projectile) and ν is the kinematic viscosity of the medium. The significance of the Reynolds number is that the flow pattern around similar shapes is identical provided that the Reynolds number is the same. For example, spheres of different diameters travelling with different velocities but with the same Reynolds number have the same flow pattern and hence the same value of the drag coefficient, C_D (see figure 3 below). For a detailed discussion of the Reynolds number, its relation to the drag coefficient and the so-called boundary layer, see the text by Kundu and Cohen (2008) or the advanced work by Schlichting and Gersten (2000).

[9] Cricket balls of course possess seams which, amongst other things, aid in 'swing' bowling. The treatment of the seam is beyond the scope of this work.

(see figure 3). The primary effect of a roughened surface is to reduce the critical Reynolds number below the value of 3×10^5 applicable to smooth spheres; however the value of C_D in the immediate sub-critical region still remains at about 0.45 (Achenbach 1972, 1974). Nevertheless it must be recognized that, for real non-smooth spheres used in ball games, there is the distinct possibility of exceeding the critical Reynolds number, particularly early in the flight, with a consequent abrupt *increase* in the drag coefficient to 0.45 as V decreases.

In addition to the complications noted above (i.e. the effect of a non-smooth surface on C_D and whether or not the critical Reynolds number is exceeded), few studies have been made of how the angular velocity, ω, of a rotating sphere affects C_D. Davies (1949) found, from wind tunnel measurements, that for a fixed wind velocity of $105 \, \mathrm{ft \, s^{-1}}$ (approximately $32 \, \mathrm{m \, s^{-1}}$ or $115 \, \mathrm{km \, h^{-1}}$), for normal 'dimpled' golf balls the drag increased nearly linearly with spin for ω in the range 0–$8000 \, \mathrm{rpm}$ (approximately $838 \, \mathrm{rad \, s^{-1}}$). His result in fact leads to the following relationship between C_D and ω:

$$C_D = 0.30 + 2.58 \times 10^{-4}\omega, \tag{4}$$

where ω is in $\mathrm{rad \, s^{-1}}$. This implies that for golf balls travelling at $105 \, \mathrm{ft \, s^{-1}}$ we are already beyond the critical Reynolds number. Davies results were obtained only for the axis of rotation *perpendicular* to the wind stream and do not provide any information regarding arbitrary spin directions relative to the wind stream. However, Schlichting and Gersten (2000, p 331) note that even for the rotation axis *parallel* to the wind stream (for which there should be no lift force), a considerable increase in the drag force occurs as the rotation speed increases. Clearly further wind tunnel measurements, aimed at determining how C_D varies with $\vec{\mathbf{V}}$ and the angular velocity vector $\vec{\boldsymbol{\omega}}$ (particularly the variation of C_D with the direction of $\vec{\boldsymbol{\omega}}$), would be useful.

If C_D were in fact not constant but varied in a known way with $\vec{\mathbf{V}}$ and $\vec{\boldsymbol{\omega}}$, it would not cause any significant complication in the numerical solution of the equations of motion to be outlined below (see sections 4 and 6).

### 2.2. The lift force with spin about an arbitrary axis

For spins *perpendicular* to the projectile velocity it is usually assumed, on the basis of experimental evidence, that the lift or Magnus force is proportional to V^2 and to act at right angles to both $\vec{\mathbf{V}}$ and $\vec{\boldsymbol{\omega}}$. The sense of direction of the lift force is given by $\vec{\boldsymbol{\omega}} \times \vec{\mathbf{V}}$. In this situation the magnitude of the lift force is usually written as

$$F_L = |\vec{\mathbf{F}}_L| = \tfrac{1}{2}\rho A C_L V^2, \tag{5}$$

where C_L is the (dimensionless) lift coefficient which is in general a function of $\omega = |\vec{\boldsymbol{\omega}}|$.

We note in passing that equation (5) represents a significant simplification of the real situation in that, amongst other things, C_L may depend on C_D (see e.g. Nathan 2008 and references therein) and under certain circumstances the Magnus force may reverse in direction, as was first observed by Briggs (1959).

It is also found experimentally that, if $\vec{\boldsymbol{\omega}}$ is *parallel* or *anti-parallel* to $\vec{\mathbf{V}}$, the lift force is zero, as is obvious from the

$$\vec{\mathbf{F}}_{\mathrm{L}} = \tfrac{1}{2}\rho A C_{\mathrm{L}} V^2 \sin\theta \cdot \hat{\mathbf{n}}$$
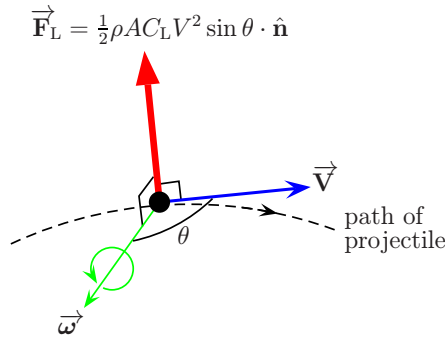
Figure 4. Schematic diagram showing the Magnus or lift force, $\vec{\mathbf{F}}_{\mathrm{L}}$, acting on a sphere travelling with velocity $\vec{\mathbf{V}}$ relative to the air and rotating with angular velocity $\vec{\boldsymbol{\omega}}$. In this diagram $\vec{\boldsymbol{\omega}}$ and $\vec{\mathbf{V}}$ are shown at an arbitrary angle of θ to each other, the direction of $\vec{\boldsymbol{\omega}}$ with respect to $\vec{\mathbf{V}}$ being completely unrestricted. It is found experimentally that if $\theta = \pm 90°$ the lift force is a maximum, whilst if $\theta = 0°$ or $\pm 180°$ the lift force is zero, the latter result being obvious on symmetry grounds. The lift force is assumed to be in the direction of $\vec{\boldsymbol{\omega}} \times \vec{\mathbf{V}}$ (i.e. perpendicular to both $\vec{\boldsymbol{\omega}}$ and $\vec{\mathbf{V}}$) and to be proportional to V^2 and $\sin\theta$. The lift coefficient, C_{L}, is a function of ω and possibly $\vec{\mathbf{V}}$.

symmetry of this situation. At first sight, at least, this would suggest that it is only the component of $\vec{\boldsymbol{\omega}}$ perpendicular to $\vec{\mathbf{V}}$ which gives rise to a lift force. The general situation is shown in figure 4, where θ is the angle between $\vec{\boldsymbol{\omega}}$ and $\vec{\mathbf{V}}$. How F_{L} in fact varies with θ for $0° < \theta < 90°$ (and for $90° < \theta < 180°$) is far from clear and depends on the details of the boundary layer surrounding the spinning sphere (see e.g. Schlichting and Gersten 2000), which is well beyond the scope of this work. However, for the purposes of the present study, in the general situation where both $\vec{\boldsymbol{\omega}}$ and $\vec{\mathbf{V}}$ have arbitrary directions, we will assume that

(i) the direction of the lift force is still given by $\vec{\boldsymbol{\omega}} \times \vec{\mathbf{V}}$, and
(ii) F_{L} varies smoothly as $\sin\theta$, since it is only the component of $\vec{\mathbf{V}}$ perpendicular to $\vec{\boldsymbol{\omega}}$ (i.e. $V\sin\theta$) which appears to give rise to the lift force.

We re-emphasize that (i) and (ii) above are assumptions, which are certainly valid if $\theta = 0°$, $\pm 90°$ or $\pm 180°$, but which need to be verified by wind tunnel experiments for other values of θ as the actual physical situation is certainly non-trivial.

With these assumptions the lift force may be expressed as

$$\vec{\mathbf{F}}_{\mathrm{L}} = \tfrac{1}{2}\rho A C_{\mathrm{L}} V^2 \sin\theta \cdot \hat{\mathbf{n}}, \tag{6}$$

where $\hat{\mathbf{n}}$ is a unit vector in the direction of $\vec{\boldsymbol{\omega}} \times \vec{\mathbf{V}}$. That is

$$\hat{\mathbf{n}} = \frac{\vec{\boldsymbol{\omega}} \times \vec{\mathbf{V}}}{|\vec{\boldsymbol{\omega}} \times \vec{\mathbf{V}}|}. \tag{7}$$

Noting that $\sin\theta$ may be written as $|\vec{\boldsymbol{\omega}} \times \vec{\mathbf{V}}|/(\omega V)$, equation (6) may be re-written as

$$\vec{\mathbf{F}}_{\mathrm{L}} = \frac{1}{2}\rho A C_{\mathrm{L}} V \cdot \left(\frac{\vec{\boldsymbol{\omega}} \times \vec{\mathbf{V}}}{\omega}\right). \tag{8}$$

Pioneering wind tunnel measurements of the Magnus effect for smooth rotating spheres were made by MacColl (1928) and surprisingly there exists little more
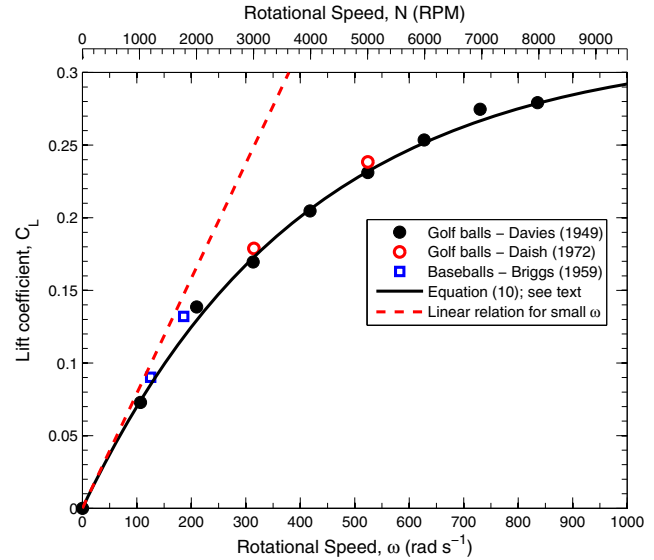
Figure 5. Lift coefficient, C_{L}, versus rotational speed, ω, for golf balls and baseballs. Filled circles represent the mean of Davies (1949) results for standard golf balls with 'dimple' and 'mesh' markings all obtained with a wind stream velocity of $105\,\mathrm{ft\,s}^{-1}$ ($115\,\mathrm{km\,h}^{-1}$). Open circles are unpublished golf ball results obtained from Daish (1972). Open squares are the mean of Briggs (1959) results for baseballs. These latter results were obtained for two rotational speeds, $N = 1200$ and $1800\,\mathrm{rpm}$, each of the two points being the mean of a number of results obtained for wind stream velocities in the range 75–$150\,\mathrm{ft\,s}^{-1}$ (82–$165\,\mathrm{km\,h}^{-1}$), the differences between the individual results being small compared with the size of the squares. The continuous curve represents equation (10) while the dashed line represents the linear approximation for low values of ω (see text). (The figure is based on figure 13.1 of Daish (1972) with some additions.)

consistent data, either for smooth or rough spheres. Some measurements of the lift coefficient, C_{L}, versus spin are shown in figure 5. In fact spins of up to at least $1000\,\mathrm{rad\,s}^{-1}$ are in practice encountered in golf, with considerably less spin occurring in other ball games (Daish 1972, p 62). The results for golf balls shown in figure 5 refer to the now standard 'dimpled' ball and an old style 'mesh' ball. These results and those for baseballs lie very close to a smooth curve[10]. Davies (1949) in fact found the following relationship for the lift force, F_{L}, to apply for golf balls:

$$F_{\mathrm{L}} = 0.064\left[1 - \exp\left(-0.000\,26N\right)\right], \tag{9}$$

where N is the rotational speed in rpm and F_{L} is in pounds weight. For Davies measurements the wind speed was fixed at $V = 105\,\mathrm{ft\,s}^{-1}$ ($115\,\mathrm{km\,h}^{-1}$).

Equating equations (5) and (9) and inserting the relevant constants ($\rho = 1.22\,\mathrm{kg\,m}^{-3}$ for air at $16\,°\mathrm{C}$ and normal pressure and a golf ball diameter of 1.68 inches) leads to the relation

$$C_{\mathrm{L}} = 3.19 \times 10^{-1}\left[1 - \exp\left(-2.48 \times 10^{-3}\omega\right)\right], \tag{10}$$

where ω is in $\mathrm{rad\,s}^{-1}$.

[10] However, for *smooth* golf balls, Davies (1949) and others find totally different results with a *negative* lift force (see section 1.3) being encountered for rotational speeds less than about $N = 5000\,\mathrm{rpm}$ ($\omega \approx 524\,\mathrm{rad\,s}^{-1}$). Although such smooth spheres are rarely encountered in practical situations, as noted previously the phenomenon of negative lift is clearly worthy of much deeper attention.

For $2.48 \times 10^{-3}\omega \ll 1$, i.e. $\omega \ll 400 \, \text{rad s}^{-1}$, this reduces to the linear relationship $C_L = 7.91 \times 10^{-4}\omega$.

We note that Briggs (1959) results for baseballs were obtained for a variety of wind stream velocities in the range $V = 75–150 \, \text{ft s}^{-1}$ which, for the same value of ω, all produced the same result for C_L within the experimental error. While equation (10) was in fact derived for a fixed value of the wind speed of $105 \, \text{ft s}^{-1}$, Briggs results support the assumption implicit in equation (10) that C_L, while dependent on ω is independent of V.

Štěpánek (1988) measured both C_D and C_L as a function of ω/V for tennis balls, with the axis of rotation perpendicular to the wind-tunnel air-stream, and Watts and Ferrer (1987) produced similar results for C_L for baseballs. Štěpánek (1988) concluded that his results were so scattered that a distinct dependence on the air stream velocity, V, could not be established. The dependence of C_L on ω together with the numerical values were similar to that shown in figure 5, although the equation he used to represent the variation differed from equation (10). He also found that C_D increased with ω, having a value of about 0.51 for $\omega = 0$, somewhat above our assumed value of 0.45, and rose to about 0.73 for $\omega/V = 0.6$.

To summarize, although it would seem reasonable to use $C_D = 0.45$ and equation (10) for C_L for the purposes of this study, there exists considerable uncertainty in their actual values, and results obtained by different workers differ considerably, illustrating the extreme difficulty in obtaining such observational data. However, if C_D were to vary with V and ω in a known way, as would occur if, for example, the critical Reynolds number were exceeded (see figure 3), or if C_L had a different functional dependence to equation (10), it would be a relatively simple matter to take this into account.

3. The effect of a wind

If $\vec{v}$ is the velocity of the projectile *relative to the chosen coordinate system* and a wind of velocity $\vec{W} = \vec{W}(x, y, z, t)$ is blowing *relative to this coordinate system*, then, as far as the drag and lift forces are concerned, it is the velocity of the projectile *relative to the air*, $\vec{V} = \vec{v} - \vec{W}$, which determines the magnitude and direction of these forces. Thus, in equations (3) and (8), $\vec{V}$ must be replaced by $\vec{v} - \vec{W}$ with the drag force being in the direction $-(\vec{v} - \vec{W})$ and the lift force in the direction $\vec{\omega} \times (\vec{v} - \vec{W})$. The general situation is shown in figure 6. Note that the direction of $\vec{\omega}$ is measured with respect to the coordinate system.

Hence, the drag force is now given by (cf equation (3))

$$\vec{F}_D = -\frac{1}{2}\rho A C_D |\vec{v} - \vec{W}| \cdot (\vec{v} - \vec{W}), \quad (11)$$

and the lift force by (cf equation (8))

$$\vec{F}_L = \frac{1}{2}\rho A C_L |\vec{v} - \vec{W}| \cdot \left\{ \frac{\vec{\omega} \times (\vec{v} - \vec{W})}{\omega} \right\}. \quad (12)$$

It may be noted from figure 6 that the presence of a wind shifts the direction of the drag force, $\vec{F}_D$, towards that of the wind velocity vector, $\vec{W}$. Physically, it is this change of direction of $\vec{F}_D$ which accounts for the projectile deviating in its flight towards the direction of the wind velocity vector.
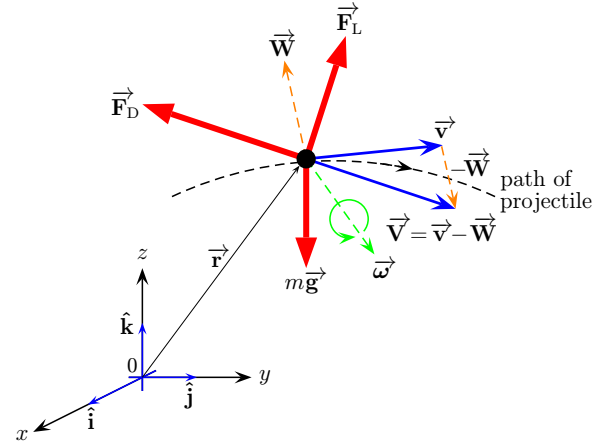
Figure 6. Schematic representation of the three forces acting on the projectile in the general situation: the drag force, $\vec{F}_D$, the lift force, $\vec{F}_L$ and the gravitational force $m\vec{g}$. $\vec{W}$ and $\vec{v}$ denote, respectively, the wind and projectile velocities relative to the coordinate system, $\vec{V} = \vec{v} - \vec{W}$ is the projectile velocity relative to the air, $\vec{\omega}$ the projectile angular velocity, $\vec{r}$ its position vector and m its mass.

4. The equations of motion in the general case

Using Newton's second law and referring to figure 6, in the presence of a wind we have

$$m\ddot{\vec{r}} = m\dot{\vec{v}} = -\frac{1}{2}\rho A C_D |\vec{v} - \vec{W}|(\vec{v} - \vec{W})$$
$$+ \frac{1}{2}\rho A C_L |\vec{v} - \vec{W}| \left[\frac{\vec{\omega} \times (\vec{v} - \vec{W})}{\omega} \right] + m\vec{g}. \quad (13)$$

Resolving this equation into components, with the z axis taken as vertically upwards, leads to

$$m\ddot{x} = -\frac{1}{2}\rho A |\vec{v} - \vec{W}| \left[C_D(v_x - W_x) \right.$$
$$\left. - C_L \left\{ \frac{\omega_y(v_z - W_z) - \omega_z(v_y - W_y)}{\omega} \right\} \right], \quad (14)$$

$$m\ddot{y} = -\frac{1}{2}\rho A |\vec{v} - \vec{W}| \left[C_D(v_y - W_y) \right.$$
$$\left. - C_L \left\{ \frac{\omega_z(v_x - W_x) - \omega_x(v_z - W_z)}{\omega} \right\} \right], \quad (15)$$

$$m\ddot{z} = -\frac{1}{2}\rho A |\vec{v} - \vec{W}| \left[C_D(v_z - W_z) \right.$$
$$\left. - C_L \left\{ \frac{\omega_x(v_y - W_y) - \omega_y(v_x - W_x)}{\omega} \right\} \right] - mg. \quad (16)$$

In equations (13)–(16)

$$\left| \vec{\mathbf{v}} - \vec{\mathbf{W}} \right| = \left[(v_x - W_x)^2 + (v_y - W_y)^2 + (v_z - W_z)^2 \right]^{1/2} \tag{17}$$

and $\omega = \left(\omega_x^2 + \omega_y^2 + \omega_z^2 \right)^{\frac{1}{2}}$.

We have also used the result that

$$
\vec{\boldsymbol{\omega}} \times \left(\vec{\mathbf{v}} - \vec{W} \right) = \begin{vmatrix} \hat{\mathbf{i}} & \hat{\mathbf{j}} & \hat{\mathbf{k}} \\ \omega_x & \omega_y & \omega_z \\ v_x - W_x & v_y - W_y & v_z - W_z \end{vmatrix}
$$

$$
= \hat{\mathbf{i}} \left[\omega_y (v_z - W_z) - \omega_z (v_y - W_y) \right]
$$

$$
+ \hat{\mathbf{j}} \left[\omega_z (v_x - W_x) - \omega_x (v_z - W_z) \right]
$$

$$
+ \hat{\mathbf{k}} \left[\omega_x (v_y - W_y) - \omega_y (v_x - W_x) \right]. \tag{18}
$$

The set of three coupled second order ordinary differential equations (equations (14)–(16)) are to be solved for x, y and z as a function of time, t, given the following conditions.

(i) Six boundary conditions, for example at time $t = 0$: $x(0)$, $y(0)$, $z(0)$ and $v_x(0)$, $v_y(0)$ and $v_z(0)$.

(ii) The components of the wind velocity, W_x, W_y and W_z, which in practical cases are likely to be constant for all values of x, y, z and t. However, if they were to vary in a known fashion with position and time, this would not complicate the method of solution unduly.

(iii) The angular velocity components, ω_x, ω_y and ω_z, assumed to be constant for all values of t. That is, the angular velocity is assumed to be constant in magnitude *and* the angular velocity vector is assumed to remain fixed in direction. Whilst there will obviously be some loss of rotational speed, in practical cases it is unlikely to be large. According to Daish (1972, p 62), much of the spin of a golf ball is retained throughout the flight, 'measurements indicating that, after a flight of 5 s, 80% or so of the spin still remains'. Clearly it would be desirable to take this loss of spin into account theoretically, however the problem is extremely complicated and appears to have been addressed only for spins orders of magnitude less than those of interest here ($\sim$100 to 1000 rad s^{-1}, see figure 5).

(iv) The values of the parameters ρ, A, C_D and C_L. For the purposes of the present paper C_D will be taken as constant and equal to 0.45 (but see section 2.1 for a further discussion of this point) and C_L will be assumed to be given by equation (10).

5. The equations of motion in simple cases

In order to provide a check of the accuracy of equations (14)–(16), we reduce them to simple cases.

5.1. Motion in the y–z plane, spin about the x-axis

Consider the case where there is zero wind (i.e. $W_x = W_y = W_z = 0$), the projectile is initially moving with a velocity confined to the y–z plane (i.e. $v_x(0) = 0$, $v_y(0) \neq 0$, $v_z(0) \neq 0$) and is spinning about the x-axis (i.e. $\omega_x \neq 0$, $\omega_y = \omega_z = 0$),
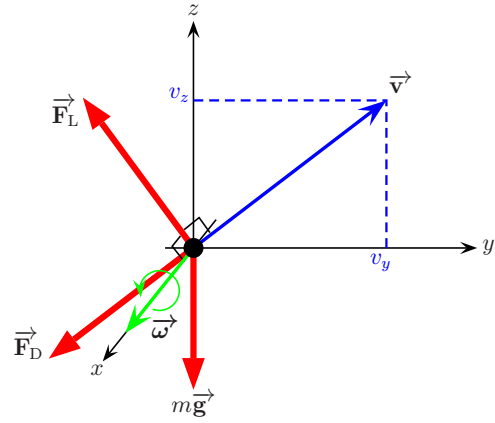
Figure 7. Projectile initial velocity vector, $\vec{\mathbf{v}}$, and angular velocity vector, $\vec{\boldsymbol{\omega}}$, for the situation where the initial velocity is confined to the y–z plane and the spin is about the x-axis, as described by equations (20)–(22). The drag force, $\vec{\mathbf{F}}_D$, is in the opposite direction to $\vec{\mathbf{v}}$ while the lift force, $\vec{\mathbf{F}}_L$, is in the direction of $\vec{\boldsymbol{\omega}} \times \vec{\mathbf{v}}$. Note that in this diagram, and also in figure 8, $\vec{\mathbf{F}}_D$, $\vec{\mathbf{F}}_L$, $m\vec{\mathbf{g}}$ and $\vec{\mathbf{v}}$ all lie in the plane of the paper while $\vec{\boldsymbol{\omega}}$ is perpendicular to the plane of the paper.

that is it possesses 'top-spin' or 'under-spin'. The situation is shown in figure 7.

Then equation (17) becomes

$$|\vec{\mathbf{v}} - \vec{\mathbf{W}}| = \left(v_y^2 + v_z^2 \right)^{\frac{1}{2}}, \tag{19}$$

and equations (14)–(16) become

$$F_x = m\ddot{x} = 0, \tag{20}$$

$$F_y = m\ddot{y} = -\tfrac{1}{2}\rho A \left(v_y^2 + v_z^2 \right)^{\frac{1}{2}} \left(C_D v_y + C_L v_z \right), \tag{21}$$

$$F_z = m\ddot{z} = -\tfrac{1}{2}\rho A \left(v_y^2 + v_z^2 \right)^{\frac{1}{2}} \left(C_D v_z - C_L v_y \right) - mg, \tag{22}$$

where F_x, F_y and F_z are the components of the resultant force on the projectile in the x, y and z directions respectively.

Reference to figure 7 and a consideration of equations (3) and (8) reveals the following. In the x direction there should be no force. In the y direction there should be a drag force (due to the y component of velocity) in the negative y direction and a lift force (due to the z component of velocity) also in the negative y direction. In the z direction there should be a drag force (due to the z component of velocity) in the negative z direction, a lift force (due to the y component of velocity) in the positive z direction and a downwards force due to gravity. This is consistent with equations (20)–(22).
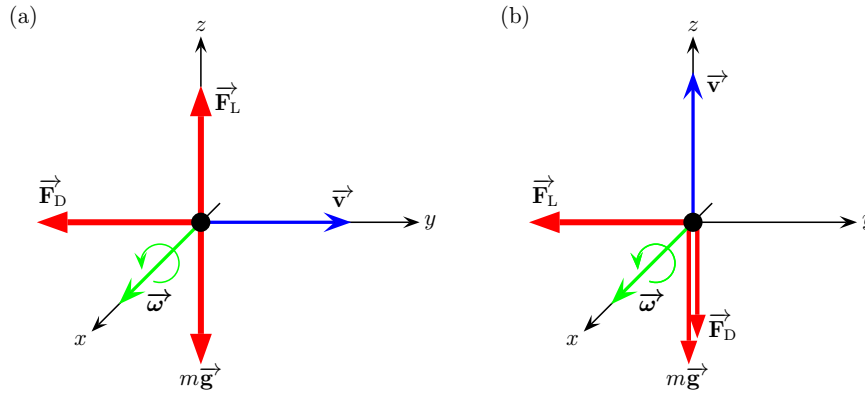
To further check the reliability of equations (14)–(16) we now divide the situation described by equations (20)–(22) into two sub-cases.

5.1.1. Motion in the y direction, spin about the x-axis. This situation, for which $v_y(0) \neq 0$, $v_x(0) = v_z(0) = 0$ and $\omega_x \neq 0$, $\omega_y = \omega_z = 0$, is shown in figure 8(a). In this case equations (20)–(22) reduce to
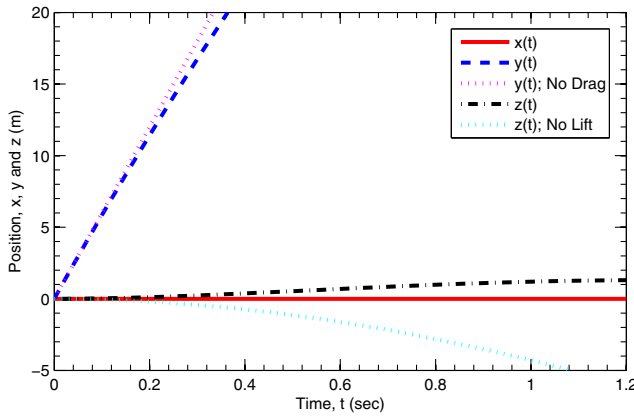
$$F_x = m\ddot{x} = 0, \tag{23}$$

$$F_y = m\ddot{y} = -\tfrac{1}{2}\rho A C_D v_y^2, \tag{24}$$

$$F_z = m\ddot{z} = \tfrac{1}{2}\rho A C_L v_y^2 - mg. \tag{25}$$

Figure 8. In (a) the initial projectile velocity, $\vec{\mathbf{v}}$, is in the y direction with spin, $\vec{\boldsymbol{\omega}}$, about the x-axis, as described by equations (23)–(25), while in (b) the initial projectile velocity is in the z direction with spin also about the x-axis, as described by equations (26)–(28).

Figure 9. Diagram illustrating trajectories appropriate to equations (23)–(25), i.e. the no-wind situation with $\omega_y = \omega_z = 0$ and $v_x(0) = v_z(0) = 0$. The curves are for a golf ball (see table 1 below) projected horizontally with $v_y(0) = 60 \, \text{m s}^{-1}$ (216 km h^{-1}) and $\omega_x = 600 \, \text{rad s}^{-1}$ (under-spin). The positions $x(t)$, $y(t)$ and $z(t)$ are shown together with two extra curves, $y(t)$ for the no-drag situation and $z(t)$ for the no-lift ($\omega_x = 0$) situation. It may be seen that the drag force reduces the y displacement, and the lift force causes a displacement in the positive z direction, consistent with equations (23)–(25).

These equations are again what one would expect on physical grounds. A projectile moving with velocity directed in the positive y direction and with angular velocity vector in the positive x direction would be expected to suffer no forces in the x direction, a drag force in the negative y direction, a lift force in the positive z direction and a gravitational force in the negative z direction, as is in fact the case in equations (23)–(25). This is illustrated in figure 9, where the trajectories have been generated using the MATLAB code to be described in section 6 below. It may be seen that the results shown in figure 9 are qualitatively consistent with the above discussion. Note, however, that strictly speaking the discussion above applies only at $t = 0$. For $t > 0$, $v_z \neq 0$ and this produces a component of the lift force in the negative y direction. This will be explored further in sections 7.2.2 and 7.2.3 in connection with a cricket ball 'drift' and 'dip'.

5.1.2. Motion in the z direction, spin about the x-axis. This situation, for which $v_z(0) \neq 0$, $v_x(0) = v_y(0) = 0$ and $\omega_x \neq 0$, $\omega_y = \omega_z = 0$, is shown in figure 8(b). In this case
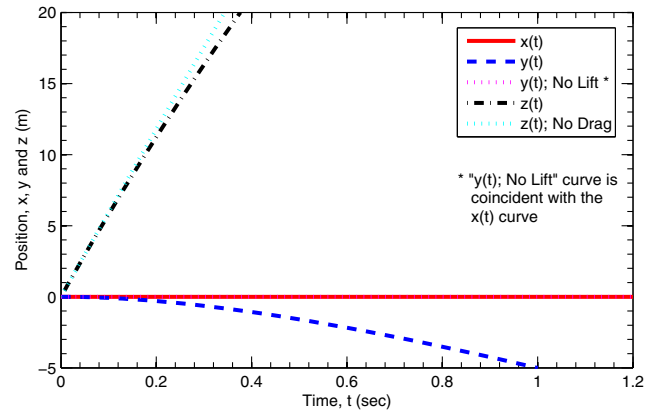
Figure 10. Diagram illustrating trajectories appropriate to equations (26)–(28), for the same parameters as in figure 9 except that $v_z(0) = 60 \, \text{m s}^{-1}$ (216 km h^{-1}) and $v_y(0) = 0$. It may be seen that the lift force causes a displacement in the negative y direction and the drag force reduces the z displacement, consistent with equations (26)–(28).

equations (20)–(22) reduce to

$$F_x = m\ddot{x} = 0, \tag{26}$$

$$F_y = m\ddot{y} = -\tfrac{1}{2}\rho A C_{\text{L}} v_z^2, \tag{27}$$

$$F_z = m\ddot{z} = -\tfrac{1}{2}\rho A C_{\text{D}} v_z^2 - mg. \tag{28}$$

On physical grounds, a projectile moving with velocity directed up the positive z-axis and with angular velocity vector in the positive x direction would be expected to suffer no forces in the x direction, a lift force in the negative y direction and a drag and gravitational force in the negative z direction, as is in fact the case in equations (26)–(28). This is illustrated in figure 10 and it may be seen that the numerically calculated trajectories are again consistent with the above discussion.

6. MATLAB implementation of the problem

The solution of the second order differential equations (14)–(16) is reasonably straightforward in MATLAB using the in-built solver ODE45[11]. Many excellent references

---

[11] For those who do not have access to MATLAB, there are equivalent open-source or free software packages available. Some examples and the websites from which they may be downloaded include: OCTAVE (http://www.gnu.org/software/octave), SCILAB (http://www.scilab.org/) and SCIPY (http://www.scipy.org/).

Table 1. Ball types and parameter values used for the illustrative model trajectories.

Ball type	Mass, m (kg)	Diameter, D (m)	Figure	Projection velocity (m s^{-1})	Elevation angle, ϕ (deg)
Golf	4.59×10^{-2}	4.27×10^{-2}	11–13	60	12
Cricket	1.59×10^{-1}	7.20×10^{-2}	15	30	25
Cricket	1.59×10^{-1}	7.20×10^{-2}	16–21	22	5

are available for its use, for example the comprehensive general text by Hanselman and Littlefield (2005), and the more specialized works of Polking and Arnold (2004) and Hunt *et al* (2005).

As is usual in MATLAB, second order differential equations are reduced to two first order equations. For example, equation (14) may be re-written as

$$\frac{dx}{dt} = v_x, \tag{29}$$

$$\frac{dv_x}{dt} = -\frac{1}{2}\frac{\rho A}{m}|\vec{v} - \vec{W}|\left[C_D (v_x - W_x) \right.$$
$$\left. - C_L \left\{ \frac{\omega_y (v_z - W_z) - \omega_z (v_y - W_y)}{\omega} \right\} \right], \tag{30}$$

and incorporation in MATLAB then follows in a straightforward manner. An extract from our code is listed in appendix B.

We point out two potential problems that we encountered:

(i) One must ensure that the differential equations include the current value of the projectile velocity (i.e. $y(2) = v_x$, $y(4) = v_y$ and $y(6) = v_z$ in the code in appendix B), and not just the initial velocity. This is important not only for the obvious reason, but also because, even though the direction of the angular velocity vector $\vec{\omega}$ is assumed to remain fixed, as the direction of the projectile velocity changes so also will the direction of both the drag and Magnus forces.

(ii) If the spin $\omega = 0$, then there is a division by zero in equation (30), which must, of course, be prevented. We accomplished this in a rather clumsy way by using an 'if/else' construction and repeating the above code with the lift force equated to zero. (If the spin is zero the entire term in braces in equation (30) will in fact be zero, leading to zero 'lift force', as expected.)

7. Illustrative model trajectories

In this section we present some examples illustrating the effects on model trajectories of the various parameters, namely (i) the drag force, (ii) the lift force and more specifically spin about an arbitrary axis and (iii) the prevailing wind. However, we emphasize that the results presented here are for illustrative purposes only, as their accuracy is dependent upon, amongst other things, the assumed values for the drag and lift coefficients, and these will depend on the nature of the surface of the ball considered.

Table 1 shows the ball characteristics, figure references and initial projection velocities and elevation angles used for the illustrative model trajectories presented below.

Table 2. Spin directions and terminology used to describe them for golf and cricket together with relevant figure references. For the purposes of this table it is assumed that the projectile is initially projected in the x–z plane with the x-axis being horizontal and the z-axis being vertically upwards. The golfer and the bowler in cricket are both assumed to be right handed. Note that the +ve and −ve signs relate to the spin sense of direction. For example, under ω_x, +ve means the spin vector, $\vec{\omega}$, is in the +ve x direction while −ve means it is in the −ve x direction.

Sport	Spin type	ω_x	ω_y	ω_z	Figure
Golf	Under-spin	0	−ve	0	11–13
	Top-spin	0	+ve	0	11
	Pure slice (side-spin)	0	0	−ve	12 and 13
	Part slice, part under-spin	0	−ve	−ve	12 and 13
	Pure hook (side-spin)	0	0	+ve	12 and 13
	Part hook, part top-spin	0	+ve	+ve	12 and 13
Cricket	No spin	0	0	0	15 and 16
	Leg-spin ('leg-break')	−ve	0	0	14
	Leg spinner's 'wrong-un'	+ve	0	0	14
	Off-spin ('off-break')	+ve	0	0	14 and 17–21
	Under-spin	0	−ve	0	–
	Top-spin	0	+ve	0	–
	Side-spin	0	0	+ve	17 and 18

Table 2 summarizes the terminology used for the different types of spin together with figure references where the terms are referred to, although trajectories for all these spin types are not necessarily included. Note that there can be confusing differences in terminology for different sports or even within the one sport. For example, for a right-hander, in golf a sliced drive resulting from side-spin curves to the right. In tennis a sliced serve, again resulting from side-spin, curves to the left and a backhand or forehand hit with under-spin and which 'lifts' is also referred to as being sliced.

7.1. Illustrative golf ball trajectories

7.1.1. A golf ball hit with under-spin or top-spin. A simple example of a golf ball struck with a driver with no spin, under-spin and top-spin is shown in figure 11, with the x-axis being taken as the direction of the drive. Under-spins of about 50 rev s^{-1} (3000 rpm or about 314 rad s^{-1}) are not uncommon with drivers Daish (1972, p 62) and in figure 11 we have used a value of $\omega = 300$ rad s^{-1} (about 2865 rpm). The under-spin causes the lift force to act upwards and not only increases the carry very dramatically, but also increases the maximum height significantly from about 6 to 12 m. The ball remains in the x–z plane since the spin axis is in the y direction, perpendicular to the velocity vector, thus producing a lift force confined to the x–z plane. Note also that a more subtle effect of the under-spin is that, because of the z component of the velocity, while the ball is rising the lift force will oppose the horizontal velocity, v_x, and when it starts to fall it will aid it. On the other hand, top-spin results in a downward lift force
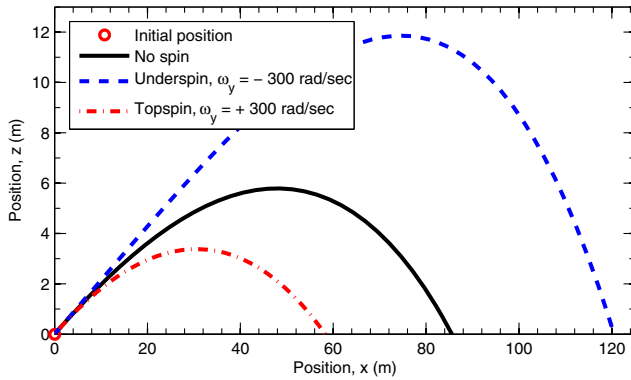
Figure 11. The effect of under-spin and top-spin on the trajectory and range of a golf ball hit with an initial speed of $60\,\mathrm{m\,s^{-1}}$ ($216\,\mathrm{km\,h^{-1}}$) and at an elevation angle of $12°$. A spin of $\omega_y = -300\,\mathrm{rad\,s^{-1}}$ corresponds to under-spin and a spin of $\omega_y = +300\,\mathrm{rad\,s^{-1}}$ corresponds to top-spin, less rarely employed in golf. It can be seen that for this particular case under-spin drastically increases the carry by about $34\,\mathrm{m}$ (about 40%) and the ball travels essentially in a straight line for the first $40\,\mathrm{m}$ or so of its path. On the other hand top-spin reduces the carry by about $28\,\mathrm{m}$ (about 33%).

decreasing the carry and maximum height dramatically. Again a subtle bi-product of top-spin is the effect on the horizontal component of velocity: while rising the combination of v_z and the lift force will increase v_x, and when it starts to fall it will reduce v_x. For both under-spin and top-spin, the effect of the lift force on v_x contributes to the shapes of the trajectories in figure 11, although the effect is relatively small because of the initial projection angle of only $12°$ elevation.

7.1.2. A golf ball hit with a slice or a hook. As a second example, consider a similar situation to the under-spin and top-spin cases of figure 11, with the same magnitude of spin as in figure 11, i.e. $\omega = 300\,\mathrm{rad\,s^{-1}}$, but with four different spin directions. The results are displayed in figure 12 and, in three-dimensional form in figure 13, together with the under-spin trajectory of figure 11, the meaning of the terms 'pure slice', 'pure hook', 'part slice' and 'part hook' having been defined in table 2. For the part slice and part hook cases, for illustrative purposes we have assumed that the spin axis is now at an angle of $45°$ to the vertical, i.e. $|\omega_y| = |\omega_z| = 212\,\mathrm{rad\,s^{-1}}$ (about 2025 rpm) and $\omega_x = 0$. Note in particular how, aside from the expected bending out of the x–z plane, the part hook ball drops quite quickly as a result of the top-spin component whereas the part slice ball rises as a result of an under-spin component causing lift.

7.2. Illustrative cricket ball trajectories

Since the terminology for cricket is quite unique and the ball trajectories can be many and varied, in figure 14 we show a schematic and exaggerated representation of the trajectory of a slow bowler's off-spin delivery together with a cricket pitch with important distances and terminology indicated. Note that the cricket pitch length is 22 yards ($20.12\,\mathrm{m}$) and, for illustrative purposes, we have shown the ball 'pitching' at about $18\,\mathrm{m}$ from the point of delivery. This latter figure is somewhat arbitrary as the point of delivery, shown as adjacent to the stumps at the bowler's end, and the point of pitching may vary considerably.
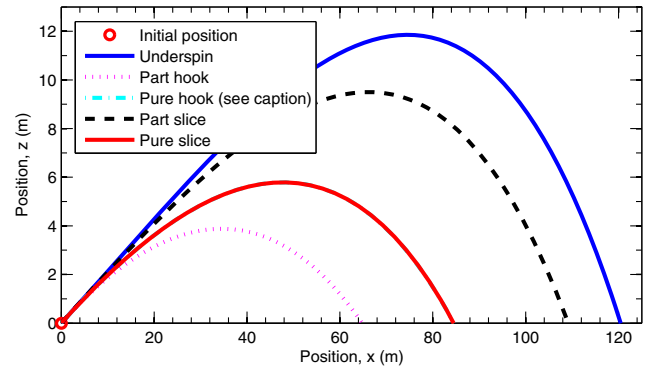
Figure 12. Showing the effects of hook and slice on the golf shot of figure 11. The various curves are as follows; under-spin: $\omega_y = -300\,\mathrm{rad\,s^{-1}}$, part hook: $\omega_y = \omega_z = +212\,\mathrm{rad\,s^{-1}}$, pure hook: $\omega_z = +300\,\mathrm{rad\,s^{-1}}$, part slice: $\omega_y = \omega_z = -212\,\mathrm{rad\,s^{-1}}$, pure slice: $\omega_z = -300\,\mathrm{rad\,s^{-1}}$, ω_x being zero in all cases. The pure hook and pure slice curves (spins purely about the vertical or z-axis) are symmetrical about the x-axis (see figure 13 below) and hence in the present diagram overlie each other. For clarity, only the pure slice curve is shown plotted here, the pure hook curve lying behind it.

7.2.1. A cricket ball thrown from the boundary with a head or tail wind. A well known trivial example is shown in figure 15. This consists of a cricket ball thrown from the boundary from a height of $1.5\,\mathrm{m}$ with a speed of $v_0 = 30\,\mathrm{m\,s^{-1}}$ ($108\,\mathrm{km\,h^{-1}}$) at an elevation angle of $\phi = 25°$ with no spin for the following cases (i) no drag force (i.e. in a vacuum), (ii) including a drag force with no wind and (iii) with a head wind of $8\,\mathrm{m\,s^{-1}}$, and finally with a tail wind of $8\,\mathrm{m\,s^{-1}}$. For the no drag situation there is an analytic solution and the trajectory is a parabola (see e.g. Halliday *et al* 2011). For this case the range is given by $R = (v_0^2/g)\sin 2\phi = 70.35\,\mathrm{m}$ and the maximum height is given by $H = (v_0 \sin\phi)^2/2g = 8.20\,\mathrm{m}$. Given that the projection height is $1.5\,\mathrm{m}$, the range and height, as given by the numerically calculated no drag trajectory shown in figure 15, is in agreement with these analytically determined values, as is the overall trajectory.

The effects of the drag force and the head and tail winds on the trajectory are qualitatively as one would expect and the ball in fact remains in the x–z plane since it was assumed to have no spin.

7.2.2. Cricket ball side-ways 'drift'. We now consider the case of a cricket ball bowled by a spin bowler with the spin about the horizontal axis (pure off-spin or leg-spin) or about the vertical axis (side-spin). Figure 16 shows the trajectory of a cricket ball bowled with (i) no spin in still air from a height of $2\,\mathrm{m}$ at $22\,\mathrm{m\,s^{-1}}$ (about $79\,\mathrm{km\,h^{-1}}$) at an angle of elevation of $5°$ and, (ii) for comparison with figures 17 and 18 below, with a spin of $150\,\mathrm{rad\,s^{-1}}$ (about 1432 rpm) about the x-axis into a headwind of $7.5\,\mathrm{m\,s^{-1}}$. It may be seen that, in the absence of a wind, the ball pitches about $18\,\mathrm{m}$ from where it was released and that the (substantial) headwind causes the ball to pitch approximately $1\,\mathrm{m}$ shorter than the no-wind situation.

Figure 17 shows the trajectories of figure 16 viewed from above, together with three other trajectories, illustrating the effect of spin and also a wind, and figure 18 shows a three-dimension representation of the trajectories. The $\omega_x = 150\,\mathrm{rad\,s^{-1}}$ curve represents off-spin (for a right hand bowler) and is perhaps the most interesting, because it illustrates the
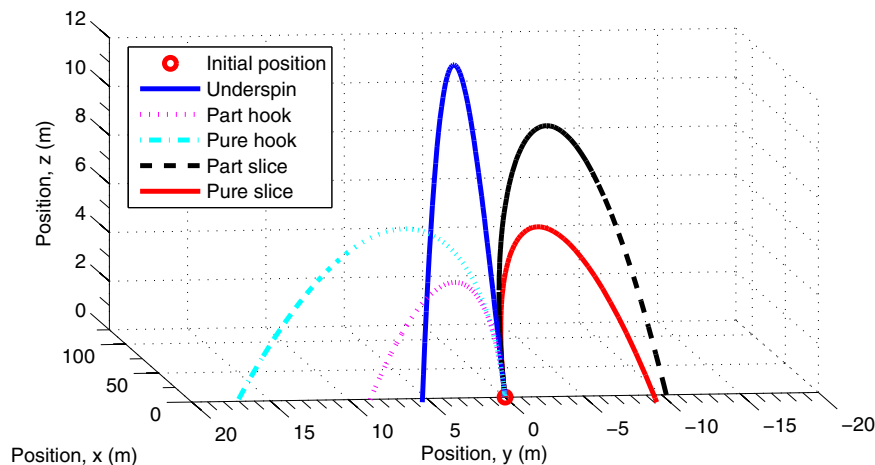
Figure 13. Showing the effects of slice and hook on the golf shot of figure 12 in three-dimensional form. Note that the pure hook and pure slice curves (spins purely about the vertical or z-axis) are symmetrical about the x-axis, but the part hook and part slice curves (spins inclined to the vertical axis by 45°) are not. The part hooked ball has a component of top-spin which causes it to dip, while the part sliced ball has a component of under-spin, which causes the ball to rise.
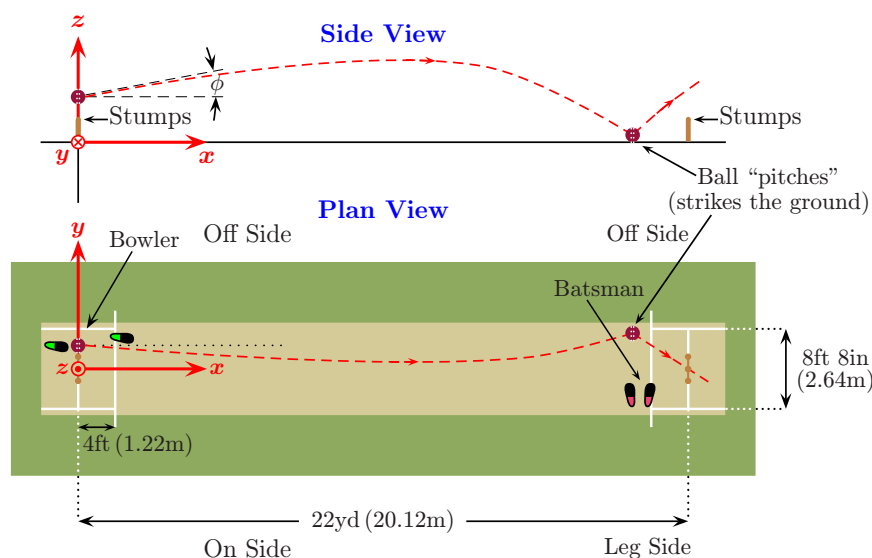

Figure 14. The upper diagram shows, as a red dashed line, a schematic trajectory of a spin-bowler's delivery in cricket as viewed from the side, the ball being bowled directly along the x-axis but at an elevation angle of ϕ (i.e. the initial velocity is confined to the x–z plane). The lower diagram shows the important features of a cricket pitch as viewed from above, assuming a right hand bowler and batsman. Also shown is the trajectory of the ball viewed from above, assuming an off-break delivery ($\omega_x = +$ve, $\omega_y = \omega_z = 0$; see table 2) and again displayed as a red dashed line (for clarity, the ball is shown being delivered from a small positive value of y). Note that an *off-break* (or a leg spinner's *wrong-un*) breaks from the off side to the leg side after pitching (i.e. towards the bottom of the page in the lower diagram), whereas a *leg-break* breaks from the leg side to the off side after pitching (i.e. towards the top of the page in the lower diagram). The lower trajectory shows the ball first drifting to the on/leg side as it rises then, as it falls, first straightening and than drifting away from the batsman towards the off side. After pitching (not discussed in this paper), the ball breaks to the leg side. See section 7.2.2 and figures 16–18 below for actual calculated trajectories up to the point of pitching for this case.

subtleties of the movement in the air of a slow bowler's spinning delivery. It may be seen that the ball first drifts slightly towards the right of the x-axis (i.e. in the $-$ve y direction, towards the leg side) *while the ball is rising* in its flight, as a result of the Magnus force arising from the z component of the velocity and the spin about the x-axis. Then, as the ball begins to *fall* and the z component of velocity reverses in direction, the Magnus force also reverses in direction and causes the ball to drift to the left of the x-axis (i.e. in the $+$ve y direction, towards the off side). That is, the ball drifts *away* from the right hand batsman in the latter parts of its flight before pitching.

A final point to note from figure 17 is that, as is to be expected, spin about the vertical axis ($\omega_z = 150\,\mathrm{rad\,s}^{-1}$)

produces a very much larger overall drift than spin purely about the horizontal axis ($\omega_x = 150\,\mathrm{rad\,s}^{-1}$). However, in the latter case movement towards the off side becomes clearly noticeable only late in the flight, even though drift to this side commences immediately the ball starts to fall, the off side drift being initially masked by the drift to the leg side as a result of the ball first rising. In the case of the example in figure 17, significant drift occurs only in the last 4 m or so of the 18 m path to pitching, and as such this 'late drift' is more likely to deceive the batsman. For the parameter values chosen the extent of the drift on pitching is approximately 1 cm, a small but not insignificant amount as it may be enough to catch the edge of the bat. Furthermore, and importantly, the head wind approximately doubles the amount of side-ways
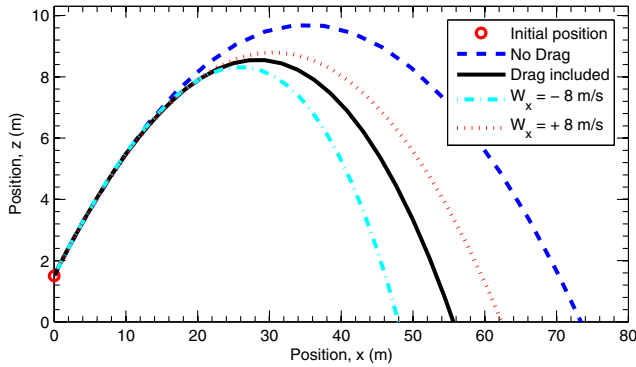
Figure 15. The effect of the drag force and the presence of a wind on the trajectory and range of a cricket ball thrown from the boundary with an initial speed of $30\,\mathrm{m\,s^{-1}}$ ($108\,\mathrm{km\,h^{-1}}$) and at an elevation angle of $25°$. It can be seen that for this particular case the drag force decreases the range by about 17 m (about 23%) and the tail and head winds of $8\,\mathrm{m\,s^{-1}}$ alter the range by a further 7 m or so (about 13%).
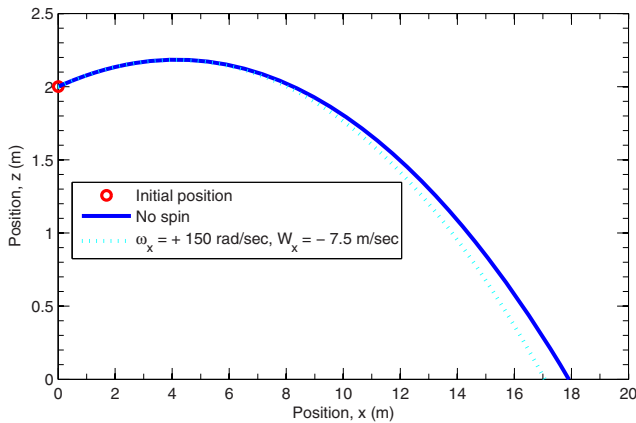

Figure 16. The trajectory of a cricket ball bowled from a height of 2 m at a speed of $22\,\mathrm{m\,s^{-1}}$ ($79\,\mathrm{km\,h^{-1}}$) and at an angle of elevation of $5°$. The solid curve represents the trajectory for no spin and with no wind present but the effects of the drag force have been included. It can be seen that the ball pitches at about 18 m from the point of delivery, the same distance as was chosen for illustrative purposes in the schematic representation of figure 14. The dotted curve is for comparison with figures 17 and 18 below (see figure 17 figure caption).

drift to approaching 2 cm, partly as a result of the steepening of the angle of decent. In fact an examination of figure 16 reveals that, for the trajectories of figures 16–18, on impact the angle of decent measured from the horizontal is only about $19°$. Very much steeper angles of decent will occur in practice and will lead to much larger side-ways drifts. If both an x and a z component of spin were included, rather than only one component as in the two extreme cases discussed above, clearly the amount of drift would be intermediate in value.

Although it is not part of this study, we note that after pitching the off-spin will cause the ball to move into the right hand batsman (i.e. in the $-ve$ y direction, towards the leg side), in the opposite direction to the drift present immediately before pitching (see figure 14).

7.2.3. Cricket ball 'lift' and 'dip' due to a cross-wind. As a final example, we consider the case shown above in figures 16–18 of off-spin ($\omega_x = +150\,\mathrm{rad\,s^{-1}}$), but with the
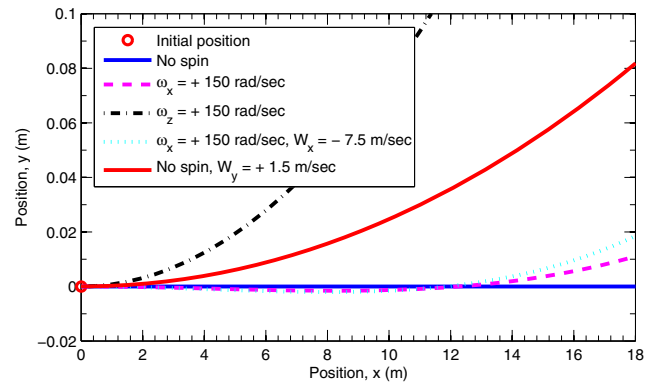

Figure 17. Looking down on the x–y plane for the trajectories shown in figure 16. The three additional trajectories shown are for (i) pure off-spin for a right hand bowler ($\omega_x = 150\,\mathrm{rad\,s^{-1}}$), (ii) pure side-spin, i.e. spin about the vertical axis only ($\omega_z = 150\,\mathrm{rad\,s^{-1}}$), and (iii) the no-spin case but with a cross-wind blowing from the leg side ($W_y = +1.5\,\mathrm{m\,s^{-1}}$). Note that these three extra trajectories fall essentially on the no-spin curve in the x–z plots of figure 16 and so were not included there.

effects of a cross-wind now included. Figure 19 shows a plan view of the trajectories for the case of no wind, $W_y = -4\,\mathrm{m\,s}$ and $W_y = +4\,\mathrm{m\,s^{-1}}$, the rather high values of the wind velocity ($14.4\,\mathrm{km\,h^{-1}}$) being chosen for illustrative purposes. The $\omega_x = +150\,\mathrm{rad\,s^{-1}}$ trajectory is identical to the corresponding curves in figures 16–18 and, as discussed previously, the ball drifts to the leg side initially as it rises and to the off side as it falls. In the presence of a wind, it may be seen from figure 19 that, not surprisingly, the ball has a significant component of its motion in the direction of the wind force vector (i.e. in the $-ve$ or $+ve$ y direction respectively).

In figure 20 we have shown the trajectories of figure 19 as viewed from the side and figure 21 displays an expanded view of figure 20 in the vicinity of the impact points. It can be seen that a wind blowing from the off side ($W_y = -4\,\mathrm{m\,s^{-1}}$) causes the ball to 'lift' slightly, or at least 'hold up' above its trajectory with no wind, whilst a wind blowing from the leg side ($W_y = +4\,\mathrm{m\,s^{-1}}$) causes the ball to drop or 'dip' slightly. Note that this motion in the vertical plane in the presence of a cross-wind is completely distinct from the vertical motion caused by top-spin or under-spin, which would occur even in the absence of a wind. If one carefully considers the direction of the Magnus force, $\vec{\omega} \times (\vec{v} - \vec{W})$, it will be seen that this modification to the motion is to be expected. The size of the effect on pitching appears to be quite small, but an examination of figure 21 shows it in fact to be $\sim \pm 4\,\mathrm{cm}$ in the z (vertical) direction for the parameter values chosen (i.e. $\omega_x = +150\,\mathrm{rad\,s^{-1}}$ and $|W_y| = 4\,\mathrm{m\,s^{-1}}$). More importantly, as shown in figure 21 this translates to the point where the ball pitches varying by $\sim \pm 14\,\mathrm{cm}$, which is large enough to potentially cause the batsman to misjudge the flight and 'spoon-up' a catch. Thus a lift or dip of even 1 cm, resulting from a modest wind of $\sim 1\,\mathrm{m\,s^{-1}}$ or $3.6\,\mathrm{km\,h^{-1}}$, may well be of significance in practice.

It might be supposed that the lift or dip is purely a result of the cross-wind giving rise to an extra path length holding the ball up in flight. However, the fact that reversal of the wind direction reverses the direction of the effect shows that this is not the case. To further demonstrate that the effect is caused by the Magnus force resulting from the interaction between
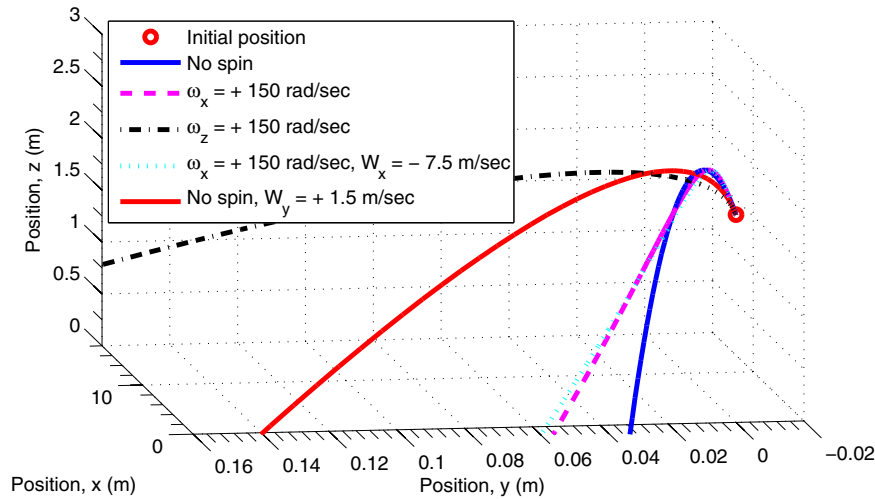
Figure 18. A three dimensional representation of the trajectories shown in figures 16 and 17.
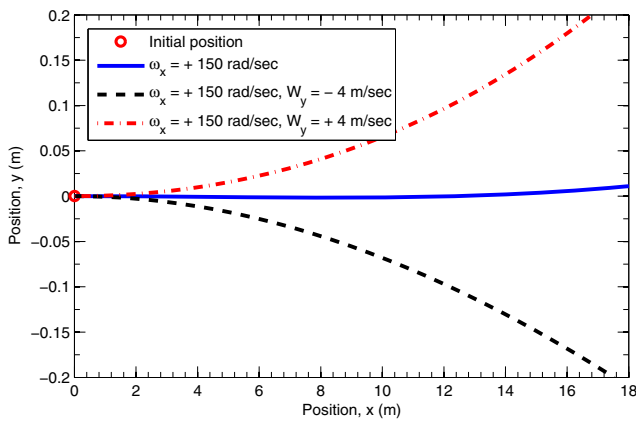

Figure 19. Diagram showing the effects of a wind blowing across the pitch in the case of a ball bowled with spin purely about the *x*-axis, in this case off-spin for a right hand bowler. Note that while there is a small net sideways drift in the positive *y* direction (i.e. towards the off side for a right hand batsman) in the case of no wind (solid curve), the presence of the cross-wind completely dominates this effect and, as expected, moves the ball in the direction of the wind.

the cross-wind operating in the *y* direction and the spin about the *x*-axis, in figure 21 we have also plotted the trajectory for the case of no spin and $W_y = +4 \, \mathrm{m \, s^{-1}}$. It may be seen that this latter curve lies essentially on the $\omega_x = 150 \, \mathrm{rad \, s^{-1}}$ curve, demonstrating that it is the spin–wind interaction which in fact causes the lift or dip.

8. Summary, conclusions and possible extensions

In this paper the equations of motion governing the trajectory of a rotating spherical projectile have been developed with the aim of applying them to 'ball-games'. The projectile is assumed to be rotating about an arbitrary axis in the presence of a wind blowing with respect to the coordinate system in an arbitrary direction. The drag and lift forces have been assumed to act in the $-(\vec{\mathbf{v}} - \vec{\mathbf{W}})$ and $\vec{\boldsymbol{\omega}} \times (\vec{\mathbf{v}} - \vec{\mathbf{W}})$ directions respectively, and both have been assumed to be proportional to $|\vec{\mathbf{v}} - \vec{\mathbf{W}}|^2$, where $\vec{\mathbf{v}}$ and $\vec{\mathbf{W}}$ are respectively the projectile and wind velocities relative to the coordinate system and $\vec{\boldsymbol{\omega}}$ is the projectile angular velocity. To the best of our knowledge the
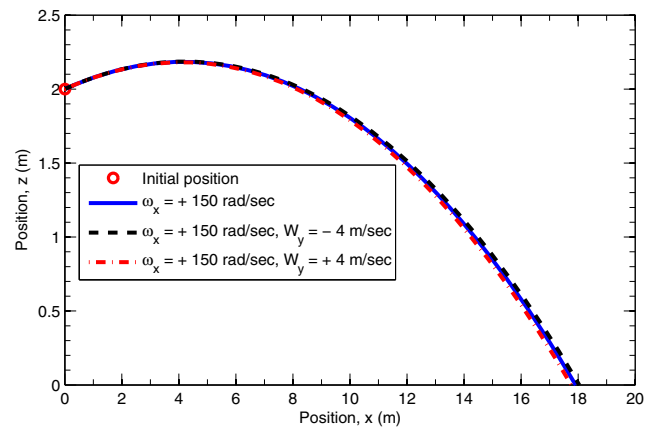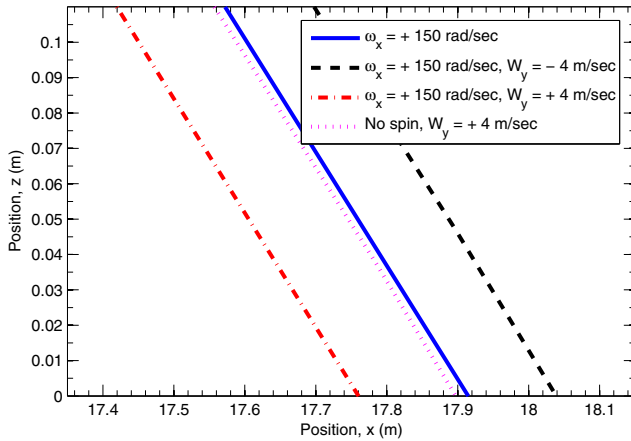

Figure 20. The trajectories of figure 19 but viewed from the side. Note how a wind blowing in the negative *y* direction (i.e. from the off side) causes the ball to 'lift' slightly whereas a wind blowing in the positive *y* direction (i.e. from the leg side) causes the ball to drop or 'dip' slightly from its normal trajectory. (See figure 21 below for a close-up of the point of impact.)

resulting equations presented here have not appeared in the literature before.

The problem has been coded in MATLAB and some illustrative model trajectories have been presented for both golf balls and cricket balls. Perhaps the most interesting result is that in cricket the lift force, generated by a slow bowler's off or leg-spin (spin about a horizontal axis, directed along the line of the pitch), can cause the ball to move in a subtle manner in the air before it pitches. Specifically:

(i) The spin can cause the ball to drift sideways in both directions while in flight. For an off-spinning delivery the drift is first to the leg and then to the off side, while for a leg-spinning delivery the reverse is true. The amount of sideways drift is increased by the presence of a head-wind (see section 7.2.2 and figures 16–18).

(ii) The presence of a cross-wind, depending on its sense of direction, may cause the off or leg spinning ball to 'lift' or 'dip' with respect to the trajectory of a ball bowled without spin, thereby altering the point of pitching significantly (see section 7.2.3 and figures 19–21).

Figure 21. The trajectories of figure 20 but viewed just before impact. It can be seen that the lift or dip in the z direction caused by the combination of the cross-wind in the y direction and the spin about the x direction is $\sim\pm 4$ cm for the parameter values chosen. The extra dotted curve is for no spin and a cross-wind of $W_y = +4\,\mathrm{m\,s^{-1}}$. The fact that it lies so close to the $\omega_x = 150\,\mathrm{rad\,s^{-1}}$ no cross-wind (solid) curve indicates that it is the Magnus force resulting from the cross-wind and the spin which causes the majority of the lift or dip, and not just the wind or spin alone.

Both of the above two motions may produce large enough deviations in the flight of the ball to aid in deceiving the batsman. No doubt these results are well known to spin bowlers the world over who are proficient in their art.

Possible extensions to this work, some of which may be used to stimulate student interest, include the investigation of:

(i) The variation of both the drag and lift coefficients, C_L and C_L, with both $\vec{\omega}$ and $\vec{V}$ for various types of balls.

(ii) The variation in the magnitude and direction of the lift force, $\vec{F}_L$, as the angle between $\vec{\omega}$ and $\vec{V}$ changes, i.e. the assumptions inherent in equation (6).

(iii) The feasibility of including *negative* lift in the equations, this phenomenon having been observed under very specific and limited conditions (see section 1.3).

(iv) The slowing down of spin as a function of time, which has not been taken into account, although for cases of practical interest measurements indicate that this is a relatively minor effect, at least for golf (Daish 1972, p 62).

(v) The possibility that the direction of $\vec{\omega}$ might change with time, particularly in the presence of a wind.

(vi) A detailed comparison of model results with observations for real projectiles used in ball-games. For example, model trajectories could be compared with observed trajectories derived from high-speed cameras such as those used by 'Hawkeye' in cricket and tennis.

(vii) The application of the equations of motion to other sports, such as tennis, soccer and baseball.

Clearly the use of extensive wind-tunnel measurements of the drag and lift coefficients for real projectiles under a variety of conditions likely to be encountered in practice is of relevance to many of the above points and would further supplement the present work.

It is hoped that the presentation of the equations of motion for this problem in the general case, together with an

Table A.1. Meaning of symbols used in this paper.

Symbol	Meaning
A	Cross-sectional area of projectile
C_D	Dimensionless drag coefficient
C_L	Dimensionless lift coefficient
d	Characteristic size of an object (used in connection with Re)
D	Projectile diameter
$\vec{\mathbf{F}}_D$	Drag force, magnitude F_D
$\vec{\mathbf{F}}_L$	Lift or Magnus force, magnitude F_L
F_x, F_y, F_z	Components of the resultant force on the projectile
$\vec{\mathbf{g}}$	Acceleration due to gravity vector, magnitude $g = 9.8\,\mathrm{m\,s^{-2}}$
m	Projectile mass
$\hat{\mathbf{n}}$	Unit vector in the direction of $\vec{\omega} \times \vec{V}$ (see below)
N	Projectile angular velocity, ω (see below), expressed in rpm
$\vec{\mathbf{r}}$	Projectile position vector, magnitude r
Re	Reynolds number (dimensionless)
$\vec{V} = \vec{v} - \vec{W}$	Projectile velocity *relative to the air* ($\vec{v}$ and $\vec{W}$ as below)
$V; V_x, V_y, V_z$	Magnitude and x, y, z components of $\vec{V}$
$\vec{v}$	Projectile velocity *relative to the chosen coordinate system*
$v; v_x, v_y, v_z$	Magnitude and x, y, z components of $\vec{v}$
$\vec{W}$	Wind velocity *relative to the chosen coordinate system*
$W; W_x, W_y, W_z$	Magnitude and x, y, z components of $\vec{W}$
θ	Angle between $\vec{\omega}$ (see below) and $\vec{V}$
ν	Kinematic viscosity of air
ρ	Density of air, taken to be $1.22\,\mathrm{kg\,m^{-3}}$
ϕ	Initial projectile elevation angle
$\vec{\omega}$	Projectile angular velocity vector
$\omega; \omega_x, \omega_y, \omega_z$	Magnitude and x, y, z components of $\vec{\omega}$ ($\mathrm{rad\,s^{-1}}$)

indication of how they may be solved in a currently available computer language and the inclusion of some illustrative model trajectories, might achieve its primary goals: (i) to cast new light on the motion of a spinning spherical projectile in the general case and (ii) to provide a vehicle for stirring the interest of students studying differential equations, particularly those interested in 'ball games'.

Appendix A

Symbols used throughout the paper are listed in table A.1.

Appendix B

An extract from the MATLAB code used for the illustrative examples.

```matlab
function dy = projectile_motion_function_v3(t,y)
%
g = 9.8;  % Acceleration due to gravity (m/s^2).
rho = 1.22; % Air density (kg/m^3).
cd = 0.45; % Drag coefficient, taken as 0.45 (dimensionless).
clcoef1 = 3.187E-1; % Multiplying constant for lift force, equation (10).
clcoef2 = 2.483E-3; % Multiplying factor for angular velocity, omega,
%   in the lift force equation, equation (10).
%
D = 7.2008E-2; % Projectile diameter (m). [Cricket ball.]
m = 1.5947E-1; % Projectile mass (kg). [Cricket ball.]
%D = 4.2672E-2; % Projectile diameter (m). [Golf ball.]
%m = 4.5926E-2; % Projectile mass (kg). [Golf ball.]
%
omx = 0.0; % x, y, z (axis) components of the initial angular
omy = 0.0; % velocity, in fact assumed to be constant for all
omz = 0.0; % time.
Wx = 0.0; % x, y and z components of the wind velocity, assumed
Wy = 0.0; % to be independent of x, y, z and t.
Wz = 0.0;
%
A = pi*D^2/4; % A is the cross-sectional area of the projectile.
kd = -0.5*rho*A*cd;
%
omega = sqrt(omx^2 + omy^2 + omz^2); % omega = angular vel. magnitude.
cl = clcoef1*(1 - exp(-clcoef2*omega)); % Lift Coeff. (dimensionless).
kl = 0.5*rho*A*cl;
%
% Dynamic section - Set up of Differential equations.
%
dy = zeros(6,1); % Sets up & initialises to zero a 6 row column vector.
%
vmw = sqrt((y(2)-Wx)^2 + (y(4)-Wy)^2 + (y(6)-Wz)^2);
% vmw is the magnitude of [vector v - vector W]; equation (17).
%
dy(1) = y(2); % x direction; equation (29)
dy(2) = (vmw/m)*(kd*(y(2)-Wx)...
 + kl*(omy*(y(6)-Wz) - omz*(y(4)-Wy))/omega); % eqs (14) & (30)
dy(3) = y(4); % y direction; cf equation (29)
dy(4) = (vmw/m)*(kd*(y(4)-Wy)...
 + kl*(omz*(y(2)-Wx) - omx*(y(6)-Wz))/omega); % equation (15); cf (30)
dy(5) = y(6); % z direction; cf equation (29)
dy(6) = (vmw/m)*(kd*(y(6)-Wz)...
 + kl*(omx*(y(4)-Wy) - omy*(y(2)-Wx))/omega) - g; %eq. (16); cf (30)
%
end;
return
```

The calling routine might use the differential equation solver 'ode45' and include:

```matlab
options = odeset('AbsTol',1e-9,'RelTol',1e-6);
[t,y] = ode45(@projectile_motion_function_v3,[t_start t_finish], ...
 [x0 vx0 y0 vy0 z0 vz0],options);
%
% x0, y0 and z0 are the co-ordinates of the point of projection.
% vx0, vy0 and vz0 are the components of the initial velocity.
```

References

Achenbach E 1972 Experiments on the flow past spheres at very high Reynolds numbers *J. Fluid Mech.* **54** 565–75

Achenbach E 1974 The effects of surface roughness and tunnel blockage on the flow past spheres *J. Fluid Mech.* **65** 113–25

Armenti A Jr (ed) 1992 *The Physics of Sports* (New York: AIP)

Briggs L J 1959 Effect of spin and speed on the lateral deflection (curve) of a baseball and the Magnus effect for smooth spheres *Am. J. Phys.* **27** 589–96

Brown F N M 1971 *See the Wind Blow* (Notre Dame, IN: The University of Notre Dame)

Carlucci D E and Jacobson S S 2008 *Ballistics: Theory and Design of Guns and Ammunition* (New York: CRC Press)

Carver M B 1979 Forsim VI: a program package for the automated solution of arbitrarily defined differential equations *Comput. Phys. Commun.* **17** 239–82

Daish C B 1972 *The Physics of Ball Games* (London: The English Universities Press)

Davies J M 1949 The aerodynamics of golf balls *J. Appl. Phys.* **20** 821–8

de Mestre N 1990 *The Mathematics of Projectiles in Sport* (Cambridge: Cambridge University Press)

French A P 1971 *Newtonian Mechanics* (New York: W W Norton) pp 507–30

Giancoli D C 2009 *Physics for Scientists and Engineers with Modern Physics* 4th edn (Upper Saddle River, NJ: Pearson/Prentice-Hall) pp 62–71

Hall E H 1903a Do falling bodies move south? Part I. Historical *Phys. Rev.* **17** 179–90

Hall E H 1903b Do falling bodies move south? Part II. Methods and results of the author's work *Phys. Rev.* **17** 245–55

Halliday D, Resnick R and Walker J 2011 *Fundamentals of Physics* 9th edn (New York: Wiley) pp 64–70

Hanselman D and Littlefield B 2005 *Mastering* MATLAB 7 (Upper Saddle River, NJ: Pearson/Prentice-Hall)

Hart D and Croft T 1988 *Modelling with Projectiles* (Chichester, Sussex: Ellis Horwood)

Housner G W and Hudson D E 1959 *Applied Mechanics* 2nd edn (London: D Van Nostrand) p 79

Hunt B R, Lipsman R L, Osborn J E and Rosenberg J M 2005 *Differential Equations with* MATLAB 2nd edn (New York: Wiley)

Klimi G 2008 *Exterior Ballistics with Applications: Skydiving, Parachute Fall, Flying Fragments* (Xlibris Corporation) (www.Xlibris.com)

Knight R D 2013 *Physics for Scientists and Engineers: A Strategic Approach with Modern Physics* 3rd edn (San Francisco, CA: Pearson) pp 91–5

Kundu P K and Cohen I M 2008 *Fluid Mechanics* 4th edn (Amsterdam: Elsevier)

MacColl J W 1928 Aerodynamics of a spinning sphere *J. R. Aero. Soc.* **32** 777–98

Magnus H G 1853 Über die Abweichung der Geschosse—about the deviation of the projectiles *Poggendorf's Ann. Phys. Chem.* **88** 1–28

Marion J B and Hornyak W F 1982 *Physics for Science and Engineering* (Philadelphia, PA: Saunders) pp 496–9

McCuskey S W 1959 *An Introduction to Advanced Dynamics* (Reading, MA: Addison-Wesley) pp 28–38

McShane E J, Kelley J L and Reno F V 1953 *Exterior Ballistics* (Denver, CO: University of Denver Press)

Mehta R D 1985 Aerodynamics of sports balls *Annu. Rev. Fluid Mech.* **17** 151–89

Moulton F R 1926 *New Methods in Exterior Ballistics* (Chicago, IL: University of Chicago Press) Re-published in 1962 under the title *Methods in Exterior Ballistics* (New York: Dover)

Nathan A M 2008 The effect of spin on the flight of a baseball *Am. J. Phys.* **76** 119–24

Newton I 1672 New theory about light and colours *Phil. Trans. R. Soc.* **80** 3075–87 1993 *Am. J. Phys.* **61** 108–12 (reprinted)

Polking J C and Arnold D 2004 *Ordinary Differential Equations using* MATLAB 3rd edn (Upper Saddle River, NJ: Pearson/Prentice-Hall)

Robinson G 1984 The motion of a rotating spherical projectile: I. The equations of motion *RAAF Academy Research Report* 153, The University of Melbourne, pp 1–22

Robinson G and Jovanoski Z 2010 Fighter pilot ejection study as an educational tool *Teaching Math. Appl.* **29** 176–92

Schlichting H 1979 *Boundary-Layer Theory* 7th edn (New York: McGraw-Hill) (translated from the German by J Kestin)

Schlichting H and Gersten K 2000 *Boundary-Layer Theory* 8th edn (Berlin: Springer) (translated from the German by K Mayes)

Scorer R S 1997 *Dynamics of Meteorology and Climate* (Chichester: Wiley-Praxis) pp 108–14

Serway R A and Jewett J W Jr 2010 *Physics for Scientists and Engineers with Modern Physics* 8th edn (Belmont CA: Brooks/Cole–Cengage Learning) pp 79–85

Spathopoulos V M 2009 A spreadsheet model for soccer ball flight mechanics simulation *Comput. Appl. Eng. Educ.* **19** 508–13

Štěpánek A 1988 The aerodynamics of tennis balls—the topspin lob *Am. J. Phys.* **56** 138–42

Synge J L and Griffith B A 1959 *Principles of Mechanics* 3rd edn (New York: McGraw-Hill) pp 138–46

Timoshenko S and Young D H 1948 *Advanced Dynamics* 1st edn (New York: McGraw-Hill) pp 94–105

Towers I N and Robinson G 2009 A model for multiple isothermal circumstellar dust shells *Phys. Scr.* **80** 015901

Van Dyke M D 1982 *An Album of Fluid Motion* assembled by M D Van Dyke (Stanford, CA: Parabolic Press)

Watts R G and Ferrer R 1987 The lateral force on a spinning sphere: aerodynamics of a curveball *Am. J. Phys.* **55** 40–4

Weidner R T and Sells R L 1973 *Elementary Classical Physics* 2nd edn (Boston, MA: Allyn and Bacon) pp 291–5

Young H D and Freedman R A 2012 *Sears and Zemansky's University Physics with Modern Physics* 13th edn (San Francisco, CA: Pearson/Addison-Wesley) pp 77–85